Title	Efficient phase-matched third harmonic generation from mid-IR to near-IR regions in a double asymmetric plasmonic slot waveguide
Author(s)	Wu, Tingting; Sun, Yunxu; Shum, Perry Ping; Shao, Xuguang; Huang, Tianye
Citation	Wu, T., Sun, Y., Shum, P. P., Shao, X., & Huang, T. (2014). Efficient phase-matched third harmonic generation from mid-IR to near-IR regions in a double asymmetric plasmonic slot waveguide. Proceedings of SPIE 9269, Quantum and Nonlinear Optics III, 9269.
Date	2014
URL	http://hdl.handle.net/10220/25124
Rights	

Efficient phase-matched third harmonic generation from mid-IR to near-IR regions in a double asymmetric plasmonic slot waveguide

Tingting Wu[a,b,c], Yunxu Sun[*a,b,c] , Perry Ping Shum[b,c], Xuguang Shao[b,c], and Tianye Huang[b,c]

[a]Harbin Institute of Technology Shenzhen Graduate School, Shenzhen, China 518055;
[b]CINTRA CNRS/NTU/THALES, UMI 3288, 50 Nanyang Drive, Singapore 637553;
[c]Nanyang Technological University, 50 Nanyang Avenue, Singapore 639798

ABSTRACT

Recent years, the research of mid-infrared (mid-IR) photonics has inspired increasingly interest due to their potential applications in a wide variety of areas, including free-space communications, chemical or biological sensors, environmental monitors, thermal imaging, IR countermeasures and medical procedures. On the other hand, third harmonic generation (THG) has been demonstrated to be a versatile tool to realize high speed optical performance monitoring of in-band OSNR and residual dispersion. The mid-IR light sources based third-order frequency conversion opens an entirely new realm of nonlinear interactions. Nevertheless, rare experimental or analytical THG modeling has been published. In this work, we theoretically investigate the possible efficient phase-matched THG in a double symmetric plasmonic slot waveguide (DAPSW) based on a mid-IR light source. Nonlinear organic material DDMEBT with third-order susceptibility of $\chi^{(3)} = 1\times10^{-19}$ m^2/V^2 is integrated into the top metallic slot region as the main slot core medium. Silicon (Si) is used to fill the bottom metallic slot region. Silver (Ag) is considered to be the metal medium due to its low Ohmic loss. The needed phase-matching condition (PMC) is satisfied between the zeroth mode at fundamental frequency (FF) and the first mode at third harmonic (TH) by appropriate designing the waveguide geometrical parameters. The associated parameters such as the width and height of the slot, pump-harmonic modal overlap, figure-of-merit (FOM), pump power and detuning have been numerically investigated in detail. Finally, the conversion efficiency comes up to 1.69×10^{-5} with pump power of 1 W and the corresponding waveguide length is 10.8 μm.

Keywords: Nonlinear optics and signal processing, Harmonic generation and mixing, Plasmonics, Integrated optics.

1. INTRODUCTION

During the past few years, mid-infrared (mid-IR) photonics have been motivating more and more increasing attentions. Accompany with the development of this special waveband, various all-optical integrated functional devices in the mid-IR region have provided potential applications, such as free-space communications, chemical or biological sensors, environmental monitors, thermal imaging, IR countermeasures and medical procedures. Especially, theories to link the mid-IR to near-IR waveband based on the nonlinear wavelength conversion have been intensively studied.[1, 2] Among the nonlinear effects, third harmonic generation (THG) has been demonstrated to be a versatile tool to realize high speed optical performance monitoring of optical signal to noise ratio (OSNR) and residual dispersion.[3] THG has also been demonstrated being a promising method in three-dimensionally storing optical data[4] and studying the biological materials.[5] Due to the development of the mid-IR communication, THG devices working in this special waveband can find more applications in the area of signal processing. Therefore, design efficient THG devices working in the mid-IR waveband is interesting and valuable.

The basic theory of the THG was developed by Armstrong *et al.*[6] and extended by Junginger *et al.*,[7] in which the analytical solutions and conversion efficiency of THG were investigated. Typically, high THG conversion efficiency depends on three crucial points, i.e. high third-order nonlinear susceptibility $\chi^{(3)}$ of the interactive material, perfect phase-matching conditions (PMC) and sufficient large figure-of-merit (FOM). To this end, different artificial structures have been proposed and explored.[8-11] However, the limitation of the small third-order susceptibility of the interactive

*sunyunxu@hitsz.edu.cn; phone: 86755 26033608; fax: 86755 26033608

Quantum and Nonlinear Optics III, edited by Qihuang Gong, Guang-Can Guo, Byoung Seung Ham, Proc. of SPIE Vol. 9269, 92690N · © 2014 SPIE
CCC code: 0277-786X/14/$18 · doi: 10.1117/12.2066964

material[8, 9] and the tiny modal overlap[10, 11] under the PMC has prevented the utilization of the THG-based devices. Although the above three key points have been predicted to be possible to obtain simultaneously by employing advanced devices or new types of nonlinear materials,[12] designing waveguides is still a challenging issue.

Recently, several types of plasmonic slot waveguide structures have been proposed, in which the light can be tightly confined in the slot region beyond the limit imposed by the laws of diffraction in dielectric medium.[13, 14] Furthermore, another advantage of plasmonic slot waveguides is that the mode effective indices can be engineered through appropriate designing the waveguide geometrical parameters. Therefore, PMC between the fundamental frequency (FF) and the generated third harmonic (TH) can be achieved via inter-modal phase-matching technique.[11] Due to these advantages, there is no surprise that plasmonic slot waveguides are of great potential to realize highly efficient THG devices. With respect to the dielectric medium in the metallic slot region, Beels *et al*. have proposed a new type of material with high third-order nonlinear susceptibility- DDMEBT polymer.[15] What's more, DDMEBT polymer is free from two-photo absorption (TPA). Then the issue becomes how to achieve large enough pump-harmonic modal overlap together with moderate linear propagation losses, namely sufficient large FOMs. Asymmetric waveguide structures have been investigated to greatly break the symmetry of the higher-order mode at TH, in which large enough pump-harmonic modal overlap is achieved.[16] Hence, asymmetric plasmonic slot waveguide structures with DDMEBT polymer integrated into the slot region could have huge potential for efficient THG.

In this paper, we propose a new double asymmetrical plasmonic slot waveguide (DAPSW) configuration with DDMEBT polymer and silicon integrated into the slot region as its core dielectric materials. We focus on the efficient THG from mid-IR (3600 nm) to near-IR (1200 nm) regions. This waveguide is able to tightly confine the electric field in the sub-wavelength slot region for both FF and TH. PMC between the zeroth mode at FF and the first mode at TH is achieved by carefully designing the waveguide geometrical parameters. By forcing the counteractive electric field distributed into the silicon slot region, the FOMs for THG are significantly enhanced. The relationships between the THG conversion efficiency and the key parameters such as slot width and height, PMC, pump-harmonic modal overlap, FOM, pump power and detuning are studied by numerical simulations in details to provide a guideline to obtain efficient THG in waveguide structure. Finally, the calculated conversion efficiency to the TH in the DAPSW is up to 1.69×10^{-5} with pump power of 1 W.

2. BASIC THG THEORY, WAVEGUIDE STRUCTURE AND PMC

2.1 Basic THG theory

To model the THG process in lossy plasmonic waveguide case, the nonlinear coupled mode theory is used. Light travelling can be described by Maxwell's curl equations with all components of the electric and magnetic fields taken into consideration,

$$\nabla\times\vec{E}(\mathrm{r},t)=-\mu_0\frac{\partial\vec{H}(\mathrm{r},t)}{\partial t} \tag{1}$$

$$\nabla\times\vec{H}(\mathrm{r},t)=\varepsilon_0\varepsilon_r\frac{\partial\vec{E}(\mathrm{r},t)}{\partial t}+\frac{\partial\vec{P}_{NL}}{\partial t} \tag{2}$$

where ε_0 and μ_0 are the linear permittivity and permeability in vacuum, ε_r is the relative permittivity . $\vec{P}_{NL}$ is the nonlinear polarization vector and $\partial\vec{P}_{NL}/\partial t$ is viewed as a source term. Assuming only two different propagating modes in the APSW, i.e. FF and TH, and neglecting their linear propagation losses at first, the total electric fields and magnetic fields at location *z* of the waveguide can be expressed as:

$$\vec{\mathrm{E}}(\vec{\mathrm{r}},t)=\sum_j\frac{\tilde{A}_j(\mathrm{z})}{2}\mathrm{Z}_0^{1/2}\vec{\mathrm{F}}_j(\vec{\mathrm{r}}_\perp)\exp[i(\beta_j\,\mathrm{z}-\omega_j t)]+c.c. \tag{3}$$

$$\vec{\mathrm{H}}(\vec{\mathrm{r}},t)=\sum_j\frac{\tilde{A}_j(\mathrm{z})}{2}\mathrm{Z}_0^{-1/2}\vec{\mathrm{G}}_j(\vec{\mathrm{r}}_\perp)\exp[i(\beta_j\,\mathrm{z}-\omega_j t)]+c.c. \tag{4}$$

in which $j=1$ refers to the case of FF, and $j=3$ refers to the case of TH, $\tilde{A}_j(\mathrm{z})$ are the slowly-varying mode amplitudes, $\vec{F}_j(\mathrm{r}_\perp)$ and $\vec{G}_j(\mathrm{r}_\perp)$ are mode profiles which have been normalized with $\frac{1}{4}\iint_{A_{NL}}(\vec{\mathrm{F}}_j\times\vec{\mathrm{G}}_j^*+\vec{\mathrm{F}}_j^*\times\vec{\mathrm{G}}_j)\cdot\hat{z}dxdy=1$. $\beta_j=\frac{\omega_j}{c}n_{eff}(\omega_j)$ are the propagation constants, $Z_0=\sqrt{\mu_0/\varepsilon_0}$ here is used to simplify the numerical calculation. $\vec{\mathrm{r}}=(x,y,z)$ and $\vec{\mathrm{r}}_\perp=(x,y)$. With the normalization, the corresponding field power can be expressed as $P_j(\mathrm{z})=\left|A_j(\mathrm{z})\right|^2$.

By using the reciprocal theorem,[14] we obtain:

$$\frac{d\tilde{A}_j}{dz}=-\frac{Z_0^{1/2}}{2}\iint_{A_{NL}}\left\langle\exp[-i(\beta_j\,\mathrm{z}-\omega_j\,\mathrm{t})]\vec{\mathrm{F}}_j^*\cdot\frac{\partial\vec{P}_{NL}}{\partial t}\right\rangle_t dxdy \tag{5}$$

where $\langle\cdots\rangle_t$ is time averaging, A_{NL} is the cross-section area of the waveguide, and the nonlinear polarization is defined as:

$$\vec{P}_{NL}=\varepsilon_0\chi^{(3)}(\vec{\mathrm{r}})(\vec{\mathrm{E}}(\vec{\mathrm{r}},t)\cdot\vec{\mathrm{E}}(\vec{\mathrm{r}},t))\vec{\mathrm{E}}(\vec{\mathrm{r}},t) \tag{6}$$

For lossy waveguides case, the complex propagation constant can be written into its real part β_j and imaginary part α_j as: $\beta=\beta_j+i\alpha_j/2$. Accordingly we define

$$A_j=\tilde{A}_j\exp(-\frac{\alpha_j z}{2}) \tag{7}$$

Substituting Eq. (7) into Eq. (6), the nonlinear polarization can be rewritten as:

$$\vec{P}_{NL}{}'=\varepsilon_0\chi^{(3)}(\vec{\mathrm{r}})(\vec{\mathrm{E}}'(\vec{\mathrm{r}},t)\cdot\vec{\mathrm{E}}'(\vec{\mathrm{r}},t))\vec{\mathrm{E}}'(\vec{\mathrm{r}},t) \tag{8}$$

where $\vec{\mathrm{E}}'(\vec{\mathrm{r}},t)=\frac{1}{2}\sum_j A_j(\mathrm{z})\,\mathrm{Z}_0^{1/2}\,\vec{\mathrm{F}}_j(\vec{\mathrm{r}}_\perp)\exp[i(\beta_j\,\mathrm{z}-\omega_j t)]+c.c.$. Substituting Eq. (8) into Eq. (5), we obtain the following nonlinear coupled-wave equation for the lossy DAPSW:

$$\frac{d\tilde{A}_j}{dz}=-\frac{Z_0^{1/2}}{2}\exp(\frac{\alpha_j z}{2})\iint_{A_{NL}}\left\langle\exp[-i(\beta_j\,\mathrm{z}-\omega_j\,\mathrm{t})]\vec{\mathrm{F}}_j^*\cdot\frac{\partial\vec{P}_{NL}{}'}{\partial t}\right\rangle_t dxdy \tag{9}$$

Then substituting Eq. (7) into Eq. (9), we finally obtain the following set of coupled-mode equations describing the THG process with linear propagation losses:

$$\frac{\partial A_1}{\partial z}=-\frac{\alpha_1}{2}A_1+i[(I_1\left|A_1\right|^2+I_2\left|A_3\right|^2)A_1+I_3(A_1^*)^2A_3e^{i\delta\beta z}] \tag{10}$$

$$\frac{\partial A_3}{\partial z}=-\frac{\alpha_3}{2}A_3+i[(I_4\left|A_1\right|^2+I_5\left|A_3\right|^2)A_3+I_6(A_1)^3e^{-i\delta\beta z}] \tag{11}$$

In which $\delta\beta=\beta_3-3\beta_1$ is the phase-mismatch, α_j are the linear propagation loss coefficients and the nonlinear coefficients I_m $(\mathrm{m}=1,2,\cdots,6)$ are defined as:

$$I_1=\frac{1}{16}z_0\cdot k_1\cdot\chi^{(3)}(\omega_1,\vec{\mathrm{r}}_\perp)\iint_{A_{NL}}(2\left|\vec{\mathrm{F}}_1\right|^4+\left|\vec{\mathrm{F}}_1^2\right|^2)dS \tag{12}$$

$$I_2=\frac{1}{8}z_0\cdot k_1\cdot\chi^{(3)}(\omega_1,\vec{\mathrm{r}}_\perp)\iint_{A_{NL}}(\left|\vec{\mathrm{F}}_1\right|^2\left|\vec{\mathrm{F}}_3\right|^2+\left|\vec{\mathrm{F}}_1\cdot\vec{\mathrm{F}}_3\right|^2+\left|\vec{\mathrm{F}}_1\cdot\vec{\mathrm{F}}_3^*\right|^2)dS \tag{13}$$

$$I_3=\frac{3}{16}z_0\cdot k_1\cdot\chi^{(3)}(\omega_1,\vec{\mathrm{r}}_\perp)\iint_{A_{NL}}(\vec{\mathrm{F}}_1^*\cdot\vec{\mathrm{F}}_3)(\vec{\mathrm{F}}_1^*\cdot\vec{\mathrm{F}}_1^*)dS \tag{14}$$

$$I_4=\frac{3}{8}z_0\cdot k_1\cdot\chi^{(3)}(\omega_3,\vec{\mathrm{r}}_\perp)\iint_{A_{NL}}(\left|\vec{\mathrm{F}}_1\right|^2\left|\vec{\mathrm{F}}_3\right|^2+\left|\vec{\mathrm{F}}_1\cdot\vec{\mathrm{F}}_3\right|^2+\left|\vec{\mathrm{F}}_1\cdot\vec{\mathrm{F}}_3^*\right|^2)dS \tag{15}$$

$$I_5 = \frac{3}{16} z_0 \cdot k_1 \cdot \chi^{(3)}(\omega_3, \vec{r}_\perp) \iint_{A_{NL}} (2\left|\vec{F}_3\right|^4 + \left|\vec{F}_3^2\right|^2) dS \tag{16}$$

$$I_6 = \frac{3}{16} z_0 \cdot k_1 \cdot \chi^{(3)}(\omega_3, \vec{r}_\perp) \iint_{A_{NL}} (\vec{F}_1 \cdot \vec{F}_3^*)(\vec{F}_1 \cdot \vec{F}_1) dS \tag{17}$$

where $k_1 = 2\pi/\lambda_1$ is the wave number. $\chi^{(3)}(\omega_j, \vec{r}_\perp)$ are the third-order nonlinear susceptibilities at any location of the waveguide. I_6 is THG nonlinear coefficient which is determined by the modal overlap between the interactive modes.

2.2 Waveguide structure and PMC

Figure 1 shows the cross-section view of the proposed DAPSW. The widths and heights of the slot are w_1 (slot width), w_2 (silicon slot width), h_1 (slot height) and h_2 (silicon slot height), respectively. Silver (Ag) is considered as the metal medium due to its low Ohmic loss and with a Drude permittivity dispersion of $\varepsilon_{Ag} = \varepsilon_\infty - f_p/[f(f + i\gamma)]$, with ε_∞ = 5, f_p = 2175 THz, and γ = 4.35 THz.[17] The parameters of the dielectric materials used in the waveguide design are as follows: The refractive index of DDMEBT and SiO_2 are obtained from,[15, 18] while the refractive index 1.9641 at 3600 nm and 2.0124 at 1200 nm are used for Si_3N_4. This double asymmetric waveguide structure (internal asymmetric: two components including DDMEBT and silicon are chosen to be embedded in the slot region, external asymmetric: different cladding and substrate materials are used) is able to greatly enlarge the pump-harmonic modal overlap. In order to couple light into and out of the DAPSW from a standard silicon waveguide, Z. Han et al. have experimentally proposed a taper-funnel mode transformer, where a coupling efficiency of 33% was realized.[19] Note that, although metal benefits from strong third-order optical nonlinearity at optical frequencies, its practical exploitation is limited by the weak penetration of the electric fields within the metal and the screening by the surface charges.[20] THG both at silver surfaces and in silver layers during our calculation is neglected since the electric field is tightly confined in the slot region, almost does not penetrate inside the metal layers and decays exponentially with distance from the metal-dielectric interface. Using this DAPSW, we investigate the conversion efficiency to the TH from mid-IR (3600 nm) to near-IR (1200 nm) regions.

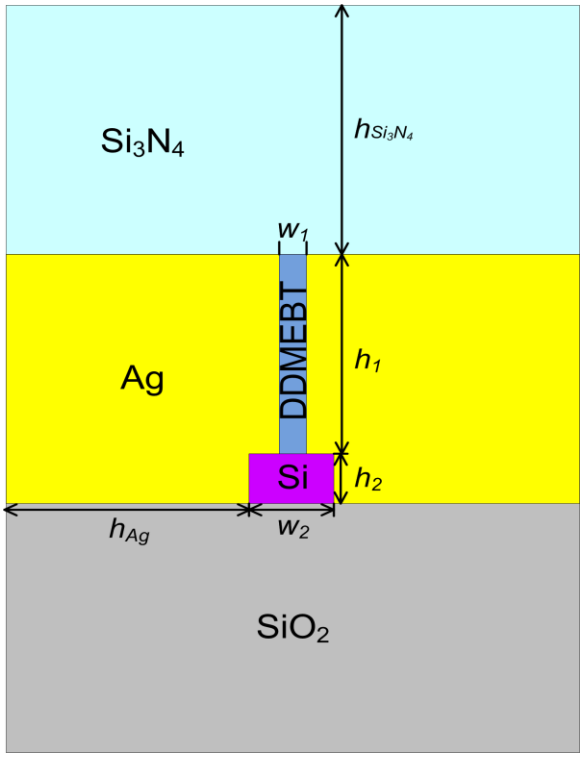

Figure 1. Cross-section view of the proposed double-asymmetric plasmonic slot waveguide (DAPSW).

The DAPSW supports SPP modes at a given wavelength with field tightly confined in the slot region due to the field discontinuity at the metal-dielectric interfaces. To further improve the THG conversion efficiency, the silicon slot is set to be wider than the DDMEBT slot. Based on the double-asymmetric waveguide structure, the enhancement of the negative part of the higher-order mode at TH is significantly reduced which results in very small counteraction effect during the calculation of the pump-harmonic modal overlap. According to our date, we use the first mode at TH to phase-match the zeroth mode at FF. During the simulation, the waveguide parameters $h_{Si_3N_4}$, h_1, h_{Ag} and w_2 are set to be 500 nm, 400 nm, 500 nm and w_1+100 nm, respectively, while the slot width w_1 and silicon slot height h_2 are adjusted to fulfill the PMC. Utilizing the finite-element-based COMSOL software, we analyze the effective mode indices of the two modes for different slot widths. Figure 2 shows the effective mode indices of the two interactive modes as a function of the silicon slot height h_2 with a fixed slot width w_1 = 40nm. As shown, the crossing point allows the PMC at 105nm in the silicon slot height. The corresponding effective mode indices of the FF and the TH are 2.7176+0.0181i and 2.7176+0.0173i, respectively.

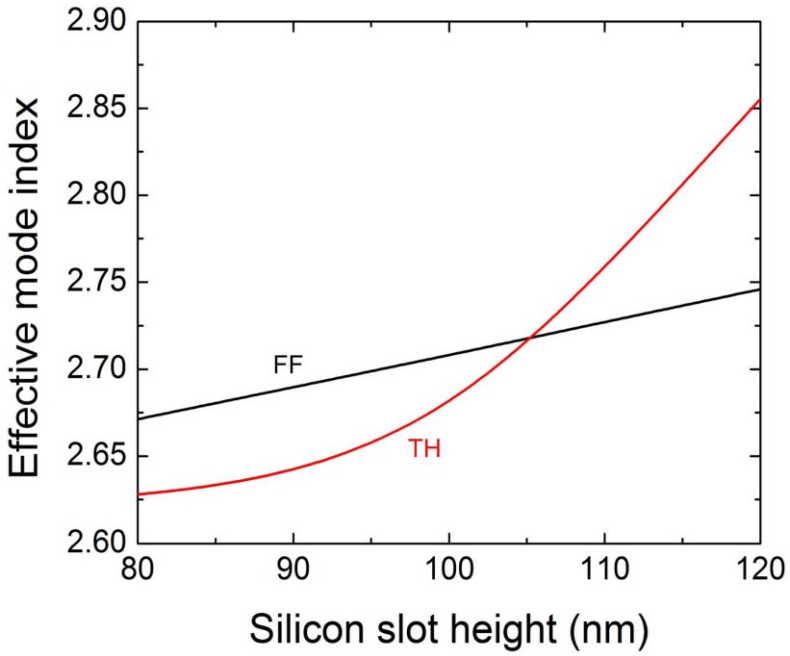

Figure 1. Effective mode indices of the zeroth mode at FF and the first mode at TH versus the silicon slot height with fixed w_1 = 40 nm, h_1 = 400 nm, w_2 = 140 nm.

3. SIMULATION RESULTS AND DISCUSSING

Figures 3(a) and 3(b) depict the corresponding 2D dominant electric field component *Ex* distributions for the zeroth mode at FF and the first mode at TH under the PMC. It can be found that, the electric components of the zeroth mode at FF are all positive while the first mode at TH preserves both positive and negative parts. We also plot the 1D electric field distributions along a *y* cutline at $x = 0$ [as the dash lines shown in Figs. 3(a) and 3(b)] in Fig. 3(c). We can see that the pump-harmonic modal overlap is large enough since the whole negative part of the first mode at TH is forced to concentrate into the thinner and wider silicon slot region. Here, the first mode at TH results from the coupling between the zeroth mode in the DDMEBT slot and the negative zeroth mode in the silicon slot. This particular field-guiding mechanism differentiates the proposed DAPSW waveguide from preciously reported planar plasmonic slot waveguides. It is known that, in common planar waveguide, the zeroth mode at FF is even symmetrical while the first mode at TH is odd symmetrical and preserves nearly equal negative and positive parts which contribute oppositely to the overlap integrals for THG leading to $I_6 \approx 0$ according to Eq. (17). One effective way to enlarge the pump-harmonic modal overlap is to reduce the negative field proportion of the TH. Therefore, we choose different cladding and substrate materials and a thinner and wider silicon slot layer to break the mode symmetry of the first mode at TH and I_6 can build

up correspondingly. This is the essential characteristic of the proposed DAPSW to increase the THG nonlinear coefficient I_6 of THG device.

Then, we analyze the influence of the slot geometry on the THG performance and choose the optimal waveguide geometry to obtain the most efficient THG among the phase-matched waveguide structures. Note that, the real and imaginary parts of $\chi^{(3)}$ are relevant to the nonlinear refractive index n_2 and the TPA coefficient α_2 by $\frac{\omega}{c} n_2(\vec{r}_\perp, \omega_j) + \frac{i}{2}\alpha_2(\vec{r}_\perp, \omega_j) = \frac{3\omega}{4\varepsilon_0 c^2 n_0^2(\omega)} \chi^{(3)}(\vec{r}_\perp, \omega_j)$.[21] We assume the nonlinear refractive index $n_2(\vec{r}_\perp, \omega_j)$ to be constant in a specific medium during the calculation since the dispersion is unknown and has always been neglected.[22, 23] The nonlinear refractive indices for DDMEBT and silicon are n_2 (DDMEBT) = 8.5×10^{-18} m^2/W,[15] n_2 (Si) = 4.5×10^{-18} m^2/W.[24] The TPA coefficient for silicon is $\alpha_2(\text{Si}) = 5.3\times10^{-12}$ m/W at TH and $\alpha_2(\text{Si}) = 0$ m/W at FF,[24] respectively. The linear absorption in the silicon slab region is neglected due to the loss-free transmission window of silicon from 1.2 to 6 μm.[25] Figure 4(a) gives the distribution of the silicon slot height versus the slot width satisfying PMC. It is seen that the silicon slot height goes up with increasing the slot width due to the weaker filed confinement. The corresponding THG nonlinear coefficient $|I_6|$ is also illustrated in Fig. 4(a). Note that, I_6 is complex due to the imaginary part of the electric field and the existence of the TPA effect. According to our calculation, increasing the absolute value of the imaginary part of the I_6, the conversion efficiency can also be enlarged. Therefore, we calculate the absolute value of the I_6, i.e. $|I_6|$. As shown in Fig. 4(a), $|I_6|$ decreases from 1022.3 to 378.4 $m^{-1}\cdot W^{-1}$. However, reducing the slot width also increases the linear propagation loss since more electronic field penetrates into the metal layers. Consequently, we define the figure-of-merit (FOM) for phase-matched THG process as:

$$\text{FOM\_FF, TH} = \frac{|I_6|}{\alpha_{FF,THF}} \tag{18}$$

where α_{FF} and α_{THF} are the linear propagation losses at FF and TH, respectively. At different PMCs, the FOMs are illustrated in Fig. 4(b). Both FOM_FF and FOM_TH decrease with increasing the slot width, which shows that the most promising slot width for efficient THG is 40 nm in this part, with corresponding h_2 = 105 nm, FOM_FF = 0.0037 $W^{-1}\cdot dB^{-1}$, and FOM_TH = 0.0013 $W^{-1}\cdot dB^{-}1$, respectively. Although the FOMs will be further improved with narrower slot, too narrow slots should not be considered due to the difficult in fabrication. Accordingly, the power leaked to the silver layers to the total input power in the optimized waveguide is also calculated to be 2.01×10^{-5} for the FF and 2.23×10^{-5} for the TH, which also demonstrates that the nonlinear process in the silver layers can be neglected.

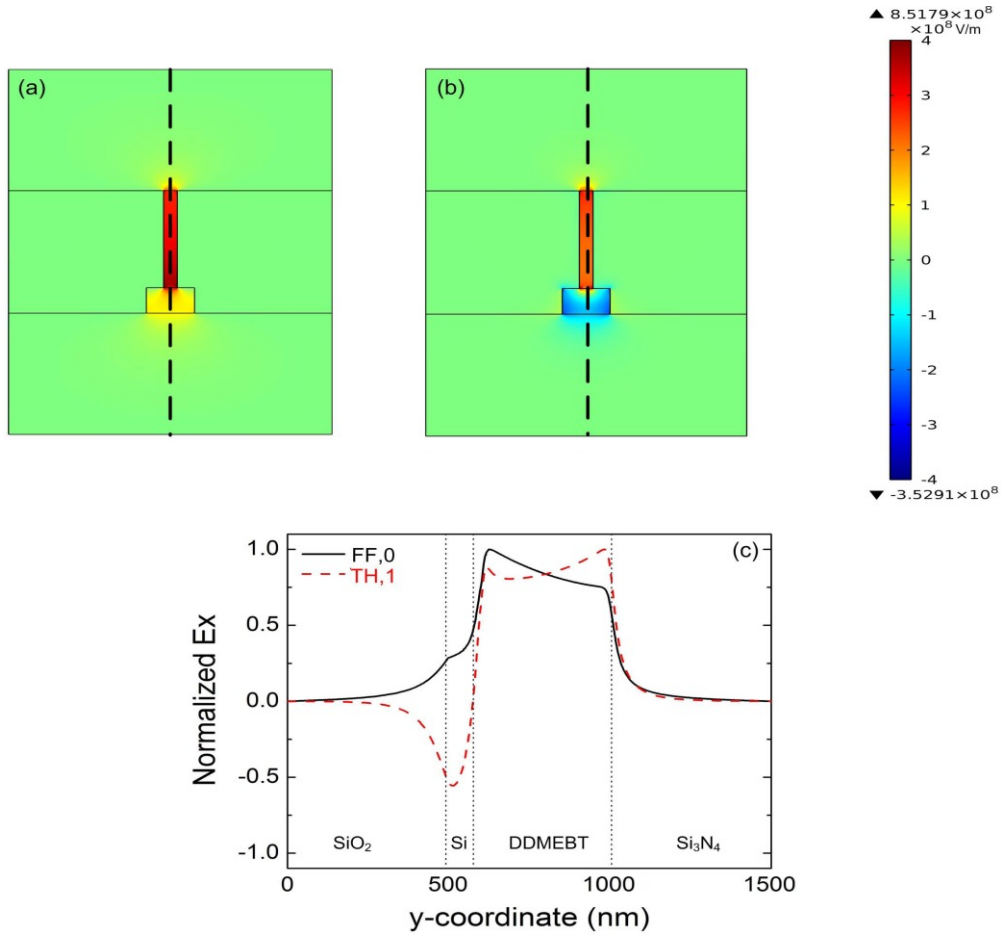

Figure 2. Major *Ex* profiles of (a) zeroth mode at FF and (b) first mode at TH; 1D *Ex* distributions of FF and TH at a cutline of (c) $x = 0$ as the dash lines plotted in (a) (b). '0' stands for the zeroth mode, '1' stands for the first mode.

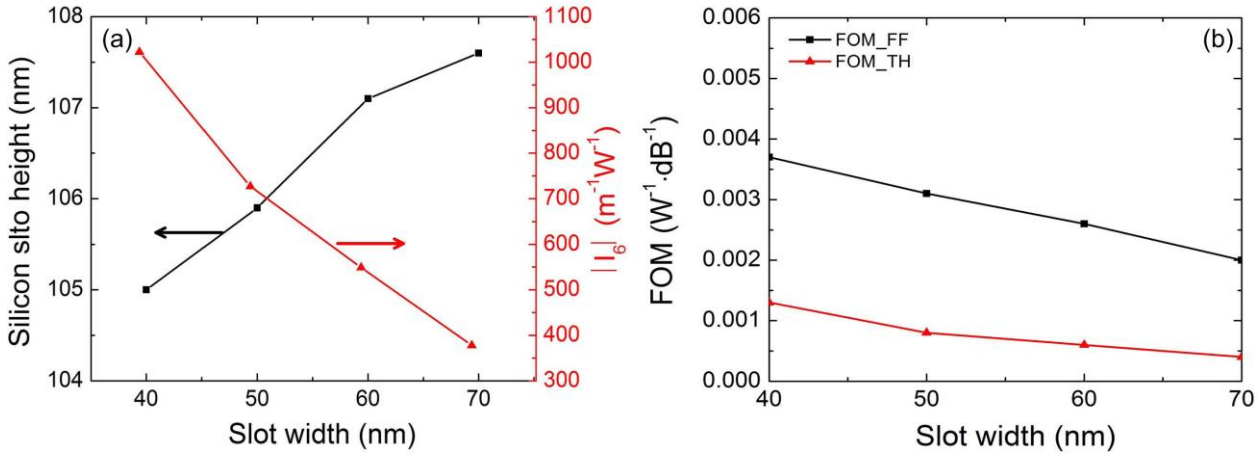

Figure 3. Silicon slot height along with the corresponding $|I_6|$ values versus the slot width satisfying PMC, (b) FOMs as a function of the slot width at different PMCs.

Finally, we calculate the power of the generated third harmonic wave and the corresponding THG conversion efficiency in the considered DAPSW for the case of Fig. 2 by numerically solving Eqs. (10) and (11) in MATLAB with Runge-Kutta method. We define the conversion efficiency as $\eta = P_3(Lp)/P_1(0)$, where $P_1(0)$ is the input pump power at FF

and Lp is the waveguide length when TH reaches its maximum output power $P_3(Lp)$. The incident power at FF is fixed to be $P_1(0)$ = 1 W. In Fig. 5(a), we give the conversion efficiency contour plot with different initial detuning constants. In this case, a maximum THG conversion efficiency is shown at an optimized detuning of $\delta\beta$ = -2190 m^{-1}. This detuning value is negatively offset from 0 to compensate for the nonlinear phase-shift during the nonlinear process. The negative detuning δβ has been demonstrated achievable by slightly perturbing the waveguide geometry with nonlinear coefficients nearly unchanged. [26] Typically in the APDSW, a variation of 1 nm to the slot width corresponds to a δβ change of ±3600 m^{-1}. Therefore, we investigate the THG efficiency with this small range of δβ. Figure 5(b) shows the power evolutions of FF and TH over the propagation distance with a detuning of -3600 m^{-1}. The pump power decreases monotonously to the nonlinear conversion process and its linear propagation loss. Harmonic power reaches its maximum value at a waveguide length of 10.8 μm, in which the THG conversion efficiency is as high as 1.69×10^{-5}. Therefore, the sufficient large FOMs illustrated in Fig. 4(b) contribute significantly in the nonlinear conversion process. To demonstrate the selected waveguide geometry is indeed the optimal waveguide structure, Fig. 5(c) gives the conversion efficiency and the correspondingly detuning as a function of the slot width. Increasing the slot width, the positive field inside the DDMEBT slot for TH decreases due to the weakened field enhancement. Therefore, the pump-harmonic modal overlap decreases accordingly which results in lower FOMs. However, the value of the detuning $\delta\beta$ increases monotonically. Since more power of FF can be transferred to TH with narrower slot, the conversion efficiency gets improved when the slot width becomes smaller.

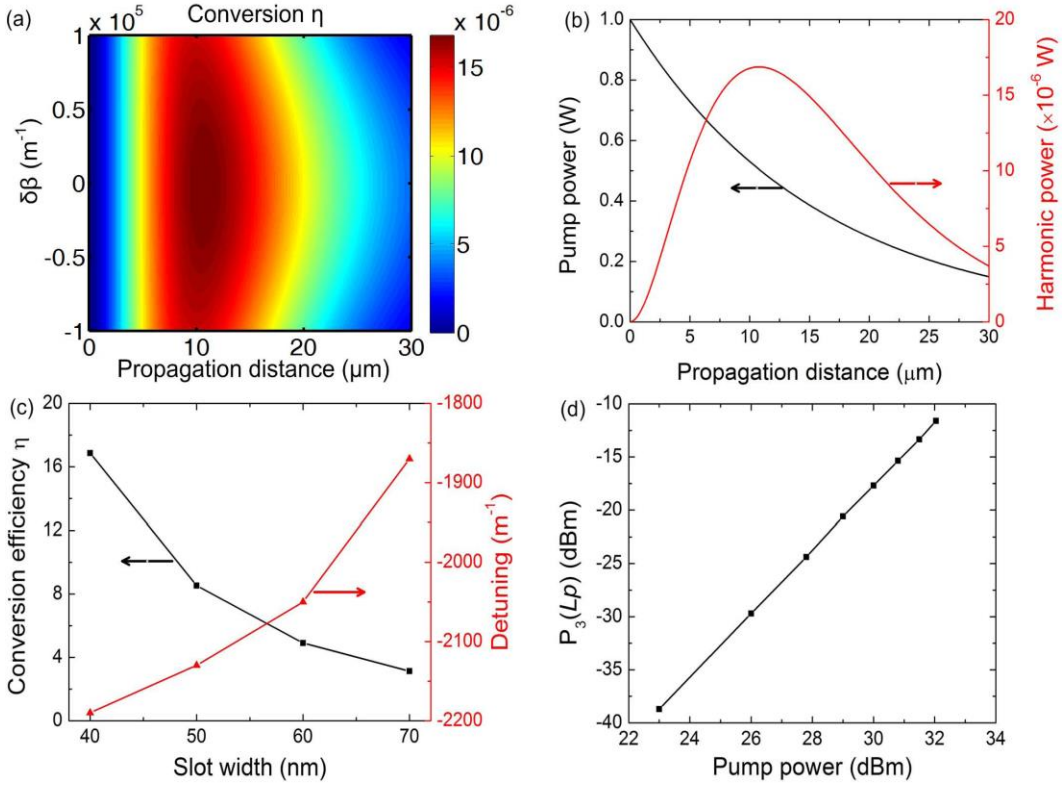

Figure 4. Fixed the pump power to be 1 W, (a) contour plot of the conversion efficiency with different $\delta\beta$ **,** (b) optical powers of FF and TH over the propagation distance with $\delta\beta$ = -3600 m^{-1}, (c) conversion efficiency and the corresponding detuning versus the slot width; (d) harmonic power versus the input pump power.

4. CONCLUSION

In conclusion, we choose to reduce the counteraction contribution of the first harmonic mode to achieve sufficient large pump-harmonic modal overlap in a double-symmetric plasmonic slot waveguide (DAPSW), in which large enough

figure-of-merits (FOMs) at fundamental frequency (FF) and third harmonic (TH) are achieved. The modal phase-matching condition (PMC) between the FF and the TH can be satisfied by appropriate designing the waveguide slot geometrical parameters. In the DAPSW, the influences of the crucial factors during the THG process have been numerically investigated in details, which provide a guideline to optimize the waveguide geometry for efficient THG in plasmonic devices.

REFERENCES

[1] Zlatanovic, S., Park, J. S., Moro, S., Boggio, J. M. C., Divliansky, I. B., Alic, N., Mookherjea, S., and Radic, S., "Mid-infrared wavelength conversion in silicon waveguides using ultracompact telecom-band-derived pump source," Nature Photon. 4(8), 561-564 (2010).

[2] Liu, X. P., Kuyken, B., Roelkens, G., Baets, R., Osgood, R. M., and Green, W. M. J., "Bridging the Mid-Infrared-to-telecom gap with silicon nanophotonic spectral translation," Nature Photon. 6(10), 667-671 (2012).

[3] Corcoran, B., Monat, C., Pelusi, M., Grillet, C., White, T. P., O'Faolain, L., Krauss, T. F., Eggleton, B. J., and Moss, D. J., "Optical signal processing on a silicon chip at 640Gb/s using slow-light," Opt. Express 18(8), 7770-7781 (2010).

[4] Canioni, L., Bellec, M., Royon, A., Bousquet, B., and Cardinal, T.,"Three-dimensional optical data storage using third-harmonic generation in silver zinc phosphate glass," Opt. Lett. 33(4), 360-362 (2008).

[5] Chu, S. W., Chen, S. Y., Chern, G. W., Tsai, T. H., Chen, Y. C., Lin, B. L., and Sun, C. K., "Studies of $\chi^{(2)}$/ $\chi^{(3)}$ tensors in submicron-scaled bio-tissues by polarization harmonics optical microscopy," Biophys. J. 86, 3914–3922 (2004).

[6] Armstrong, J. A., Bloembergen, N., Ducuing, J., and Pershan, P. S., "Interactions between light waves in a nonlinear dielectric," Phy. Rev. 127(6), 1918-1923 (1962).

[7] Junginger, H., Puell, H., Scheingraber, H., and Vidal, C., "Resonant third-harmonic generation in a low-loss medium," IEEE J. Quantum Electron. 16(10), 1132-1137 (1980).

[8] Carmon, T., and Vahala, K. J., "Visible continuous emission from a silica microphotonic device by third-harmonic generation," Nature Phys. 3(6), 430-435 (2007).

[9] Lee, T., Jung, Y., Codemard, C. A., Ding, M., Broderick, N. G. R., and Brambilla, G., "Broadband third harmonic generation in tapered silica fibres," Opt. Express 20(8), 8503-8511 (2012).

[10] Bencheikh, K. , Richard, S. , Melin, G, , Krabshuis, G. , Gooijier, F. , and Levenson, J. A. ,"Phase-matched third harmonic generation in highly germanium-doped fiber," Opt. Lett. 37(3), 289-291 (2012).

[11] Huang, T., Shao, X., Wu, Z., Lee, T., Sun, Y., Lam, H. Q., Zhang, J., Brambilla, G., and Shum, P. P., "Efficient one-third harmonic generation in highly Germania-doped fibers enhanced by pump attenuation," Opt. Express 21(23), 28403-28413 (2013).

[12] Afshar, S. V., Lohe, M. A., Lee, T., Monro, T. M., and Broderick, N. G. R., "Efficient third and one third harmonic generation in nonlinear waveguides," Opt. Lett. 38(3), 329-331 (2013).

[13] Zhang, J., Cassan, E., Gao, D.,and Zhang, X., "Highly efficient phase-matched second harmonic generation using an asymmetric plasmonic slot waveguide configuration in hybrid polymer-silicon photonics," Opt. Express 21(12), 4876-14887 (2013).

[14] Ruan, Z., Veronis, G., Vodopyanov, K. L., Fejer, M. M.,and Fan, S., "Enhancement of optics-to-THz conversion efficiency by metallic slot waveguides," Opt. Express 17(16), 13502-13515 (2009).

[15] Beels, M. T., Fleischman, M. S., Biaggio, I., Breiten, B., Jordan, M., and Diederich, F., "Compact TCBD based molecules and supramolecular assemblies for third-order nonlinear optics," Opt. Mater. Express 2(3), 294-303 (2012).

[16] Wu, T., Sun, Y., Shao, X., Shum, P. P., and Huang, T., "Efficient phase-matched third harmonic generation in an asymmetric plasmonic slot waveguide," Opt. Express 22(15), 18612-18624 (2014).

[17] Johnson, P. B., and Christy, R. W., "Optical constants of the noble metals," Phys. Rev. B, vol. 6, no. 12, pp. 4370-4379, 1972.

[18] Malitson, H. "Interspecimen comparison of the refractive index of fused silica," J. Opt. Soc. Am. 55(10), 1205-1208 (1965).

[19] Han, Z., Elezzabi, A. Y.,and Van, V., "Experimental realization of subwavelength plasmonic slot waveguides on a silicon platform," Opt. Lett. 35(4), 502-504 (2010).

[20] Ginzburg, P., Hayat, A., Berkovitch N., and Orenstein, M., "Nonlocal ponderomotive nonlinearity in plasmonics," Opt. Lett. 35(10), 1551-1553 (2010).

[21] Lin, Q., Painter, O. J., and Agrawal, G., "Nonlinear optical phenomena in silicon waveguides: Modeling and applications," Opt. Express 15(25), 16604-11644 (2007).
[22] Ning, T., Hyvarinen, P., Pietarinen, H., Kaplas, T., Kauranen, M., and Genty, G., "Third-harmonic UV generation in silicon nitride nanostructures," Opt. Express 21(2), 2012-2017 (2013).
[23] Li, G. X., Li, T., Liu, H., Li, K. F., Wang, S. M., Zhu, S. N., and Cheah, K. W., "Spectral analysis of enhanced third harmonic generation from plasmonic excitations," Appl. Phys. Lett. 98(26), 261909 (2011).
[24] Tsang, H. K., and Liu, Y., "Nonlinear optical properties of silicon waveguides," Semicond. Sci. Technol. 23(6), 064007 (2008).
[25] Hawkins, G. J., "Spectral characteristics of infrared optical materials and filters," Ph.D. thesis (University of Reading, 1998).
[26] Richard, S., "Second-harmonic generation in tapered optical fibers," J. Opt. Soc. Am. B 27(8), 1504-1512 (2010).